PCCP

ROYAL SOCIETY OF CHEMISTRY

PAPER

View Article Online
View Journal | View Issue

Cite this: *Phys. Chem. Chem. Phys.*, 2024, **26**, 14071

Host–guest interaction induced room-temperature phosphorescence enhancement of organic dyes: a computational study†

Xiaoli Luo, Yi Zeng, Haoran Wei and Xiaoyan Zheng *

To achieve the effective regulation of organic room temperature phosphorescence (RTP) in supramolecular systems, the elucidation of host–guest interactions in RTP is of vital importance. Herein, we employed two organic dyes (PYCl and PYBr) and their four host–guest complexes with CB[6] and CB[7] and explored the mechanism of host–guest interaction induced RTP enhancement using quantum mechanics/molecular mechanics (QM/MM) approach. For the two organic dyes, we found that the better RTP performance of PYBr than PYCl is attributed to intersystem crossing (ISC) augmentation induced by the heavy atom effect. Binding to CB[6] through host–guest interactions can simultaneously accelerate the radiative decay process by increasing the transition dipole moment of $T_1 \rightarrow S_0$ ($\mu_{T_1 \rightarrow S_0}$), block the nonradiative decay process, and promote the ISC process, eventually leading to a remarkably boosted RTP. Upon complexation, the conversion of S_1 from $^1(n, \pi^*)$ to $^1(\pi, \pi^*)$ is key to $\mu_{T_1 \rightarrow S_0}$ enhancement; reduced reorganization energies reflect the suppression of the nonradiative decay process by restricting the rotation of rings A and B in organic dyes. In addition, the promoted ISC process is due to the activation of more ISC channels between S_1 and high-lying triplet states with large spin–orbital coupling constants and small energy gap. The case of CB[7]-type complexes is much different, because of the extremely large cavity size of CB[7] for encapsulation. This work proposes the mechanism of host–guest interaction-induced RTP enhancement of organic dyes, thus laying a solid foundation for the rational design of advanced RTP materials based on supramolecular assemblies.

Received 29th February 2024,
Accepted 12th April 2024

DOI: 10.1039/d4cp00891j

rsc.li/pccp

Introduction

Luminophores with ultralong organic room temperature phosphorescence (RTP) have attracted the attention of many scientists because of their wide range of applications in optoelectronics,[1–3] biological imaging,[4,5] anti-counterfeiting,[6,7] data encryption,[8] *etc.*[9,10] Organic RTP materials with their high exciton utilization rate, low energy consumption and environmental friendliness have become a promising green and energy-saving optical energy source.[11–13] However, the phosphorescence quantum yield (PQY) of organic dyes is quite low under ambient conditions because of the weak spin–orbit coupling (SOC) between the excited singlet and triplet states[14] and rapid nonradiative decay of triplet excitons by molecular motions.[15]

In general, there are two efficient ways to achieve high-performance RTP. One is to accelerate the intersystem crossing (ISC) process and generate sufficient triplet excitons by introducing heavy halogen atoms[16] or other groups with heteroatoms (O, N, S, and P).[17–19] The other is stabilizing triplet excitons and suppressing the nonradiative decay channel from the lowest triplet state (T_1) to the ground state (S_0) *via* crystallization,[20] H-aggregation,[21] host–guest complexation,[22] *etc.*[23–25] Especially, host–guest complexation, where the macrocyclic host encapsulates guest molecules through weak non-covalent interactions, can effectively stabilize triplet excitons by suppressing the non-radiative decay process and promote RTP.[26,27] For example, the generation of efficient RTP for L-bromo-naphthalene was attributed to the host–guest complexation between β-cyclodextrin and L-bromo-naphthalene.[28] Both cucurbit[7]uril (CB[7]) and cucurbit[8]uril (CB[8]) can induce the phosphorescent emission of quinoline compounds by forming host–guest complexes at a 1 : 1 ratio under high pH.[29] The phosphor moiety modified β-cyclodextrin (bromo-2-naphthol-β-cyclodextrin) also exhibits phosphorescent emission owing to hydrogen bond interactions between bromo-2-naphthol and the hydroxyl group of β-cyclodextrin.[30] Organic dyes PYCl and PYBr formed by 4-(4-bromophenyl)-*N*-methylpyridinium (PY^+) with chlorine or bromine ions as counterions showed a PQY of 2.6% and 4.6% with blue and yellow emission, respectively.[31] Both PYCl and PYBr exhibit phosphorescence

Key Laboratory of Cluster Science of Ministry of Education, Beijing Key laboratory of Photoelectronic/Electro-photonic Conversion Materials, School of Chemistry and Chemical Engineering, Beijing Institute of Technology, Beijing, 100081, China. E-mail: xiaoyanzheng@bit.edu.cn

† Electronic supplementary information (ESI) available. See DOI: https://doi.org/10.1039/d4cp00891j

enhancement upon complexation with CB[6] with PQY increased to 81.2% and 72.9%, respectively. However, when binding to CB[7], the corresponding changes of PQY are negligible.[31] Although the phosphorescence enhancement induced by host–guest complexation is universal experimentally, the fundamental relationship among molecular configuration, molecular packing and photophysical properties remains rare, largely due to the limited temporal and spatial resolution of the experimental techniques at the current stage.

Theoretically, it is reported that the boosted RTP of terephthalic acid from the gas phase to crystal is related to the transition nature conversion of S_1 from $^1(n, \pi^*)$ to $^1(\pi, \pi^*)$ induced by the intermolecular electrostatic interactions.[32] The molecular descriptors for molecular designs of efficient RTP were also proposed theoretically to elucidate the key role of the excited state components ($n\pi^*/\pi\pi^*$) on phosphorescent performance.[33] The triphenylethylene derivatives achieve RTP through the radiative decay process from the high-lying triplet state,[34] *etc.*[35,36] However, theoretical studies on elucidating the underlying mechanism of the RTP enhancement induced by host–guest interactions are still rare. Therefore, it is crucial to explore the host–guest interaction-induced RTP enhancement mechanism and provide effective clues for the precise design of organic dyes with good performance on the RTP materials by regulating host–guest interactions.

In this work, we take two organic dyes PYCl and PYBr and their host–guest complexes with CB[6] and CB[7] as examples, including PYCl/CB[6], PYBr/CB[6], PYCl/CB[7] and PYBr/CB[7], to systematically explore the mechanism of host–guest interaction induced RTP enhancement by hybrid quantum mechanics/molecular mechanics (QM/MM) approach, see Fig. 1a. It was found that the PQY of PYBr is higher than that of PYCl, because of the more effective ISC process induced by heavy atom effect. Upon complexation with CB[6], the significantly increased PQY is cooperatively contributed by the boost of phosphorescent radiative transition, the acceleration of ISC from S_1 to triplet states, as well as the restriction of non-radiative decay process, because of the host–guest interactions (Fig. 1b). While binding to CB[7], the change of PQYs from pure guests is almost neglectable, due to weak host–guest interactions between guests and CB[7] with a too large cavity size. Our theoretical protocol is applicable to other host–guest complexes, which provide a theoretical foundation for the rational design of advanced RTP materials.

Computational methods

The crystal structures of PYCl, PYBr, and PYCl/CB[6] were inherited from the experiment.[31] The crystal structure of PYBr/CB[6] was obtained by substituting chlorine ions with bromine ions based on the unit cell of PYCl/CB[6]. The crystal structures of PYCl/CB[7] and PYBr/CB[7] were constructed by placing the PY^+ moiety inside the center of the CB[7] cavity[37] and adding counterions chlorine ion or bromine ion accordingly. The setup crystal structures of four host–guest complexes (PYCl/CB[6], PYBr/CB[6], PYCl/CB[7] and PYBr/CB[7]) were firstly optimized by PBE functional with Grimme's D3 correction[38] using Vienna *Ab initio* Simulation Package (VASP).[39] The energy cutoff and the convergence threshold for self-consistent-field iteration were set to 400 eV and 10^{-4} eV, respectively. The optimization would be terminated if the force on each atom was smaller than 0.05 eV $Å^{-1}$. Both lattice parameters and atomic positions of all host–guest complexes were fully optimized and their lattice parameters are summarized in Fig. S1 and Table S1 (ESI†).

The photophysical properties of PYCl and PYBr and their four host–guest complexes (PYCl/CB[6], PYBr/CB[6], PYCl/CB[7] and PYBr/CB[7]) were calculated using the QM/MM calculations in Gaussian 16 software package.[40] For each system, the supercell was extracted from the bulk crystal to build the QM/MM model.[31] It is worth mentioning that in the crystals of PYCl and PYBr, there are also some water molecules existing. In the setup of the QM/MM model for pure guest systems (PYCl and PYBr), one of the central PYCl or PYBr in the supercell was selected as the QM region, while the others (including water and other PYCl or PYBr molecules) were set as the MM region (Fig. 2). As for host–guest complexes, one central PY^+ without counterion in the supercell was chosen as the QM region, and the remaining part (including other PY^+, anions and cucurbituril molecules) was treated as the MM region. The selection of the QM region takes into account the distance between the PY^+ and counterion. As shown in Fig S2a (ESI†), it can be seen that the distance between the Br atom of the PY^+ and the anion (Cl^-) is about 2.99 Å, which is less than the sum of van der Waals radii of chlorine (1.80 Å) and bromine (1.95 Å) atoms. However, for PYCl/CB[6], the closest distance of the Cl^- to the plane of PY^+ is 7.64 Å (Fig. S2b, ESI†); for PYCl/CB[7], the closest distance from the PY^+ plane to the chloride ion is 13.39 Å (Fig. S2c, ESI†), which is much larger than the sum of their van der Waals radii. Moreover, PY^+ and chloride ions are separated by the host. Therefore, only one PY^+ without counterion was chosen as the QM part for host–guest complexes. The QM region provides critical information about the electronic excited state, while the MM region includes important corrections from environments.

To find the proper density functional that could reproduce the experimental phosphorescent spectra, a series of density functionals, including TPSSh,[41] B3LYP,[42] BMK,[43] and M06-2X[44] combined with 6-31G** basis set were selected to optimize the PYBr structure at S_0 and T_1 by the QM/MM model. The phosphoresce emission spectrum of PYBr was also calculated based on the optimized structure at T_1. It was found that the excitation energy 2.44 eV at T_1 was calculated based on the BMK/6-31G** level was close to that of the experimental[31] value, indicating the calculation at the BMK/6-31G** level was optimal (Fig. S3, ESI†). For all systems, the QM region was treated by BMK/6-31G** and the MM region was handled by the universal force field (UFF).[45,46] During geometry optimization, only molecules in the QM region were allowed to fully relax and the others in the MM region were frozen. There are no symmetry constraints of geometry optimization. Normal-mode analysis was performed for each optimized structure to guarantee no

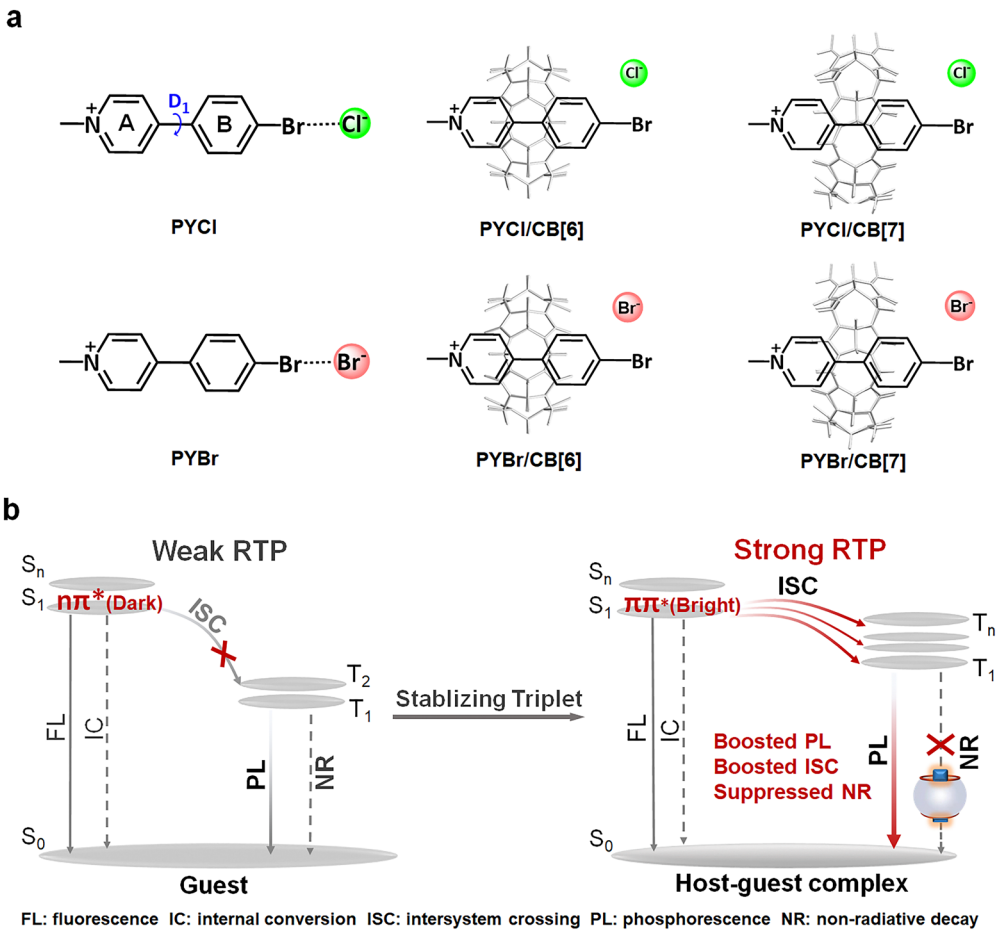

Fig. 1 (a) The chemical structures of two guests (PYCl and PYBr) and four host–guest complexes (PYCl/CB[6], PYBr/CB[6], PYCl/CB[7] and PYBr/CB[7]) with key structural parameters labeled. (b) Proposed mechanism of host–guest interaction induced RTP enhancement.

imaginary frequency. The electrostatic embedding scheme with QM polarization was adopted,[47] the partial charges of atoms for all systems were generated by the restrained electrostatic potential fitting (RESP) method.[48]

Based on the optimized electronic structures by the QM/MM calculations, the oscillator strength and transition dipole moment of $T_1 \rightarrow S_0$ ($f_{T_1\text{-}S_0}$ and $\mu_{T_1 \rightarrow S_0}$) for each system were calculated using the Dalton 2020.1 program.[49,50] The SOC constant was evaluated using Orca 4.1.4[51] at the BMK/6-31G** level. The reorganization energy (λ), which measures the extent of intramolecular electron-vibration coupling of the studied system, was obtained through four-point calculations according to the adiabatic potential (AP) energy surface.[52]

Results and discussions

Intermolecular interactions and geometric configurations

The intermolecular interactions play key roles in determining the photophysical properties of organic dyes in the aggregated state. For the organic dyes, the intermolecular interactions are similar, they both have hydrogen bonds and π–π interactions. Hydrogen bonds are formed between the H atoms of phenyl and pyridine of PYCl and PYBr molecules and the hydroxyl group of water. Additionally, hydrogen bonds are formed between the H atom of water and the anions of PYCl and PYBr molecules. The π–π interactions are formed among adjacent benzene rings or pyridine rings of guests (Fig. S4, ESI†). Upon complexation with CB[6] or CB[7], the intermolecular host–guest interactions become more complicated. CB[6] possesses a unique hydrophobic cavity and two completely symmetric polar ports that can form strong hydrogen bonds with guests (PYCl and PYBr). For example, the C–H···O (1.476–2.407 Å) formed between the inlet carbonyl part of CB[6] and C–H bonds of PYCl (Fig. S5a, ESI†). These intermolecular interactions also exist in PYBr/CB[6] (Fig. S5b, ESI†). In contrast with PYCl/CB[6], the host–guest interactions of PYCl/CB[7] are much weaker, reflected by the larger C–H···O bonding distance ranging from 2.259 to 2.527 Å (Fig. S5c and d, ESI†). That is because PYCl and PYBr are not well fit for the large cavity of CB[7], leading to a relatively loose encapsulation of guests in the CB[7] cavity. To better illustrate the intermolecular interactions, the independent gradient model (IGM) analysis and the binding energy calculations were performed for the host–guest complexes. The hydrogen bond interactions, van der Waals interactions, and steric repulsions are presented in blue, green, and red,

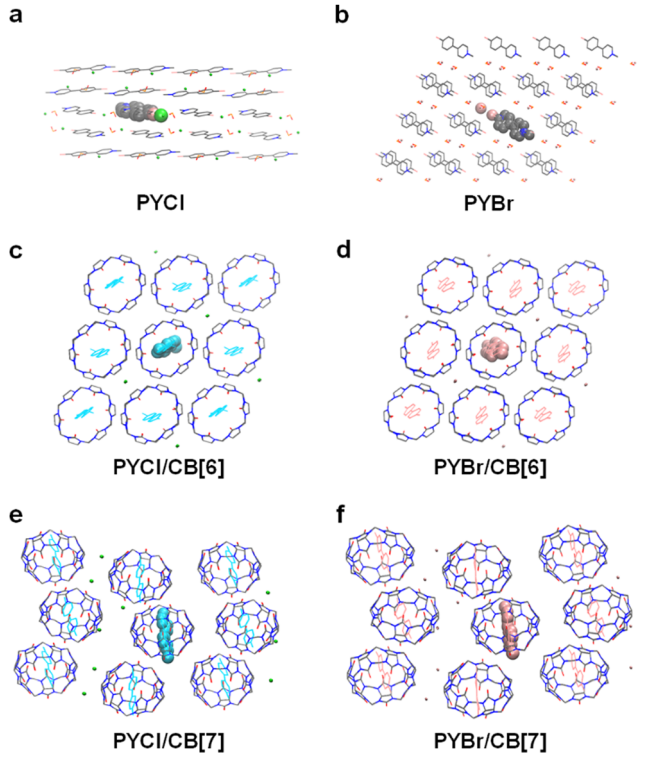

Fig. 2 QM/MM models of guests (a) PYCl (b) PYBr. Single centered PYCl or PYBr molecule is defined as the QM region, whereas all the remaining molecules (water and other PYCl or PYBr molecules) act as the MM region. The QM/MM models of host–guest complexes (c) PYCl/CB[6], (d) PYBr/CB[6], (e) PYCl/CB[7], and (f) PYBr/CB[7]. Single centered PY^+ is defined as the QM region, whereas all the remaining molecules (other PY^+, anions and cucurbituril molecules) are set as the MM region.

respectively (Fig. 3a). In IGM analysis, a broader distribution and more concentrated color region indicate stronger intermolecular interactions. It is obvious that the intermolecular interactions between CB[6] and both guests (PYCl and PYBr) are stronger than those of CB[7], especially the hydrogen bond and van der Waals interactions, supported by the more broadened and concentrated blue and green regions in Fig. 3a. In addition, the binding energies of PYCl/CB[6] and PYBr/CB[7] are also more negative than those of the CB[7]-type complexes (Fig. 3a).

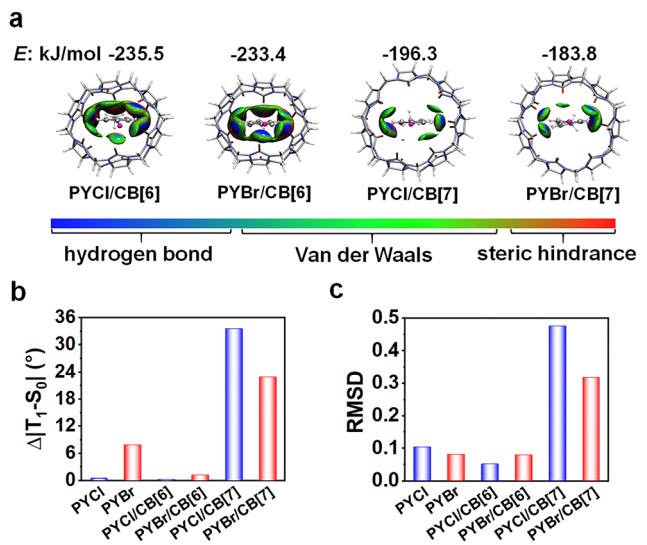

Fig. 3 (a) The calculated binding energies between guests and hosts, and the intermolecular interactions of the host–guest complexes obtained *via* IGM analysis. (b) The dihedral angle (D_1) changes and (c) the RMSD values between the T_1 and S_0 of the studied systems.

The intermolecular host–guest interactions may influence the geometric structures of the organic dyes accordingly. The optimized geometric structures of the two guests (PYCl and PYBr) and four complexes (PYCl/CB[6], PYBr/CB[6], PYCl/CB[7] and PYBr/CB[7]) at S_0 and T_1 based on QM/MM models were analyzed. The key structural parameters and their structural modifications between S_0 and T_1 $|\Delta(T_1–S_0)|$ of the six systems were extracted and summarized in Fig. 3b and Tables S2, S3 (ESI†). It is found that the geometrical changes $|\Delta(T_1–S_0)|$ of bond lengths (within 0.08 Å) and bond angles (within 2°) of all systems are negligible (Tables S2 and S, ESI†3), while the corresponding structural changes in the dihedral angle D_1 between the rings A and B are important. As shown in Fig. 3b, the $|\Delta(T_1–S_0)|$ of D_1 for PYCl and PYBr are 0.38° and 7.78°, which are larger than those of the host–guest complexes PYCl/CB[6] (0.13°) and PYBr/CB[6] (0.95°), respectively, but are much smaller than those in PYCl/CB[7] (33.42°) and PYBr/CB[7] (22.81°). Thus, the rotation of rings A and B is significantly restricted after binding to CB[6] due to strong host–guest interactions, the case of CB[7]-type complexes is opposite. Furthermore, the overall structural difference between S_0 and T_1 of all studied systems was quantified by the root mean square displacement (RMSD). It was found that the RMSD value of PYBr (0.0803 Å) is smaller than that of PYCl (0.1038 Å), indicating less structural changes of PYBr than PYCl upon excitation to T_1 (Fig. 3c and Fig. S6, ESI†). Binding to CB[6], the RMSD values were largely reduced to 0.0503 and 0.0791 Å for PYCl/CB[6] and PYBr/CB[6], respectively, while the corresponding RMSD values increased to 0.4744 Å and 0.3168 Å for PYCl/CB[7] and PYBr/CB[7], respectively. It is implied that the vibrational motions of PYCl and PYBr are significantly restricted after binding to CB[6], but activated upon binding to CB[7].

Properties of the low-lying excited states

To obtain a deep understanding of the excited state properties, the information of the transition nature of S_1 and T_1 for the six systems was demonstrated through natural atomic orbital (NAO) analysis[53] (Table S4, ESI†). As shown in Fig. 4a and b, it was found that the transition nature of PYCl and PYBr of S_1 was assigned as (n, π*), with HOMO located at the anion and LUMO delocalized on the entire molecule (Fig. 4a). Upon complexation, the transition nature of S_1 for all studied host–guest complexes belongs to the (π, π*) feature, with HOMO and LUMO delocalized on the entire molecule (Fig. 4a and Fig. S7, ESI†). The transition nature of S_1 changes from ^{1}(n, π*) in pure guest to ^{1}(π, π*) in host–guest complexes. As shown in Fig. S8 and Table S5 (ESI†), the transition orbitals of PYCl of S_1, S_2, S_3 and S_4 are mainly assigned by HOMO → LUMO, HOMO−1 →

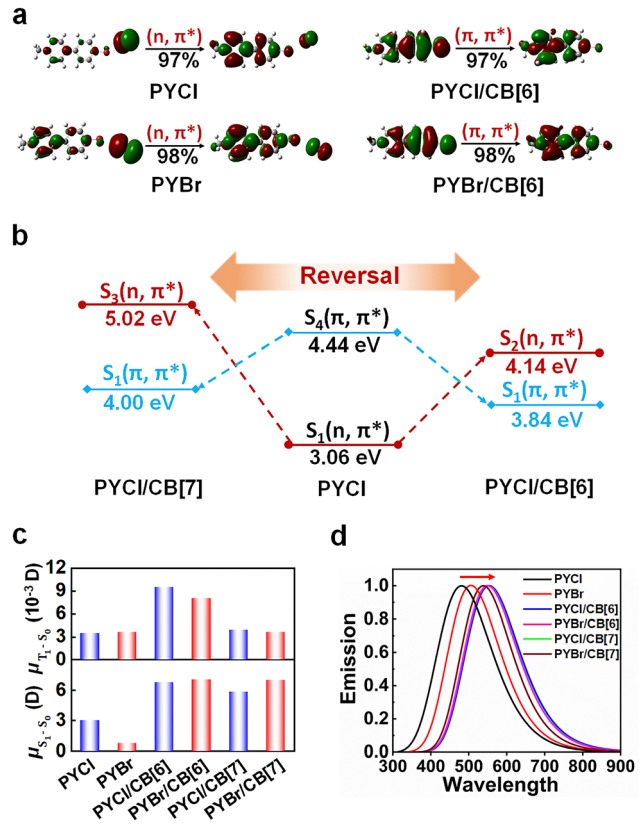

Fig. 4 The frontier molecular orbitals at S_1-geometry of (a) PYCl, PYBr, PYCl/CB[6] and PYBr/CB[6]. (b) The energy levels of key transition orbitals and the corresponding transition properties of PYCl, PYCl/CB[6] and PYCl/CB[7] at singlet. (c) The transition dipole moment (μ) and (d) the calculated phosphorescence spectra of the studied systems in crystalline state based on the BMK/6-31G** level.

LUMO, HOMO−2 → LUMO and HOMO−3 → LUMO transitions, respectively. While S_1, S_2, and S_3 are in (n, π*) character, and S_4 belongs to (π, π*). For PYCl/CB[6], the transition nature of S_1 is dominated by the HOMO → LUMO transition with (π, π*) feature, and S_2 exhibited the HOMO−1 → LUMO transition with (n, π*) feature. The transition property of PYCl/CB[7] is similar to that of PYCl/CB[6] with S_1 and S_2 in (π, π*), while S_3 belongs to (n, π*). Upon host–guest complexation, the transition nature of the lowest excited state is inverted due to the blueshift of (n, π*) and the redshift of (π, π*). For example, the excitation energy of ^{1}(n, π*) increased from 3.06 eV in PYCl to 4.14 eV in PYCl/CB[6], while the excitation energy of ^{1}(π, π*) reduced from 4.44 eV in PYCl to 3.84 eV in PYCl/CB[6] (Fig. 4b). While for the transition natures of T_1, all studied systems predominantly bear the (π, π*) feature and are distributed over the entire skeleton (Fig. S9, ESI†).

The transition nature of the S_1 state is changed from (n, π*) to (π, π*) after complexation, directly influencing the excited state behavior, especially for the oscillator strength (f) and transition dipole moment (μ). From PYCl to PYCl/CB[6], the oscillator strength between S_0 and S_1 ($f_{S_1-S_0}$) significantly increases, and the corresponding oscillator strength between T_1 and S_0 ($f_{T_1-S_0}$) increases by one order of magnitude (Table S6, ESI†), which is beneficial for phosphorescent radiative transition. While the corresponding $f_{T_1-S_0}$ of PYCl/CB[7] only slightly increases compared to PYCl. The case of PYBr is similar. In general, the enhanced phosphorescence in crystalline is related to the increased electric transition dipole moment ($\mu_{T_1\to S_0}$) of $T_1 \to S_0$.[32] The $\mu_{T_1\to S_0}$ were estimated qualitatively by the equation of $\mu_{T_1\to S_0} \propto \frac{\xi_{T_1-S_n}\mu_{S_n\to S_0}}{\Delta E_{T_1\to S_n}}$, where $\mu_{S_n-S_0}$ is the electric transition dipole moment between the intermediate singlet (S_n) and S_0, $\xi_{T_1-S_n}$ is the SOC constants between S_n and T_1, and $\Delta E_{T_1-S_n}$ is the energy difference between T_1 and S_n. For simplicity, only considering n = 1 in the equation, namely, $\mu_{T_1\to S_0}$ consists of transition $T_1 \to S_1$ *via* spin–orbit coupling followed by spin and electric dipole-allowed $S_1 \to S_0$ transition. From PYCl to PYCl/CB[6], $\mu_{T_1-S_0}$ exhibits a remarkable growth from 0.0035 D to 0.0095 D, due to the constant value of $\xi_{T_1-S_1}/\Delta E_{T_1-S_1}$ and the increase of $\mu_{S_1-S_0}$ from 3.02 to 6.78 D (Fig. 4c and Table S6, ESI†). Similar to PYCl, $\mu_{T_1\to S_0}$ of PYBr also increases obviously when binding to CB[6] due to the cooperative decrease of $\xi_{T_1-S_1}/\Delta E_{T_1-S_1}$ and increase of $\mu_{S_1-S_0}$. While for both PYCl and PYBr, the enhancement of $\mu_{T_1-S_0}$ are not observed in PYCl/CB[7] and PYBr/CB[7] complexes. Therefore, the significant increase of $\mu_{T_1-S_0}$ from pure guests to CB[6]-type complexes are dominant by the increase of $\mu_{S_1-S_0}$ induced by the reversal of the transition nature of the S_1 state from (n, π*) to (π, π*), while the $\mu_{T_1-S_0}$ is basically constant in CB[7]-type complexes.

The calculated phosphorescent emission of host–guest complexes are all red-shifted compared to that in the corresponding pure guest molecule, consistent with experimental results[31] (Fig. 4d and Table S7, ESI†), supported by the reduced HOMO–LUMO energy gap at T_1 from 5.1 eV for PYCl to 4.7 eV for PYCl/CB[6] and 4.8 eV for PYCl/CB[7] (Fig. S10, ESI†). A similar variation trend of the HOMO–LUMO energy gap was also observed in PYBr and its host–guest complexes.

Decay process of excited states

Radiative decay, non-radiative decay and ISC are three key decay processes that determine phosphorescent efficiency. The radiative rate constant (k_P) of phosphorescence is estimated from the Einstein radiative relationship: $k_P = f_{T_1-S_0}\Delta E_{T_1-S_0}{}^2/1.499$ for a two-level system,[54,55] where $f_{T_1-S_0}$ is the oscillator strength and $\Delta E_{T_1-S_0}$ is the vertical excitation energy of $T_1 \to S_0$ based on the T_1-geometry, in units of cm^{-1}. It is found that the k_P of PYCl and PYBr are similar, but they are much smaller than those of host–guest complexes (Fig. 5a). After complexation, the k_P increases about one order of magnitude from 28 of PYCl to 208 s^{-1} of PYCl/CB[6], because the increase of $f_{T_1-S_0}$ is larger than the decrease of $\Delta E_{T_1-S_0}$ (Tables S7 and S8, ESI†). Similarly, the k_P of PYBr also increases approximately by one order of magnitude upon complexation. While binding to CB[7], the k_P is almost constant, because the increase of $f_{T_1-S_0}$ offsets the reduction of $\Delta E_{T_1-S_0}$ (Tables S7 and S8, ESI†).

The non-radiative decay process is governed by the electron-vibration coupling, which is quantified by the reorganization energy (λ). The increase of λ can aggrandize the non-radiative

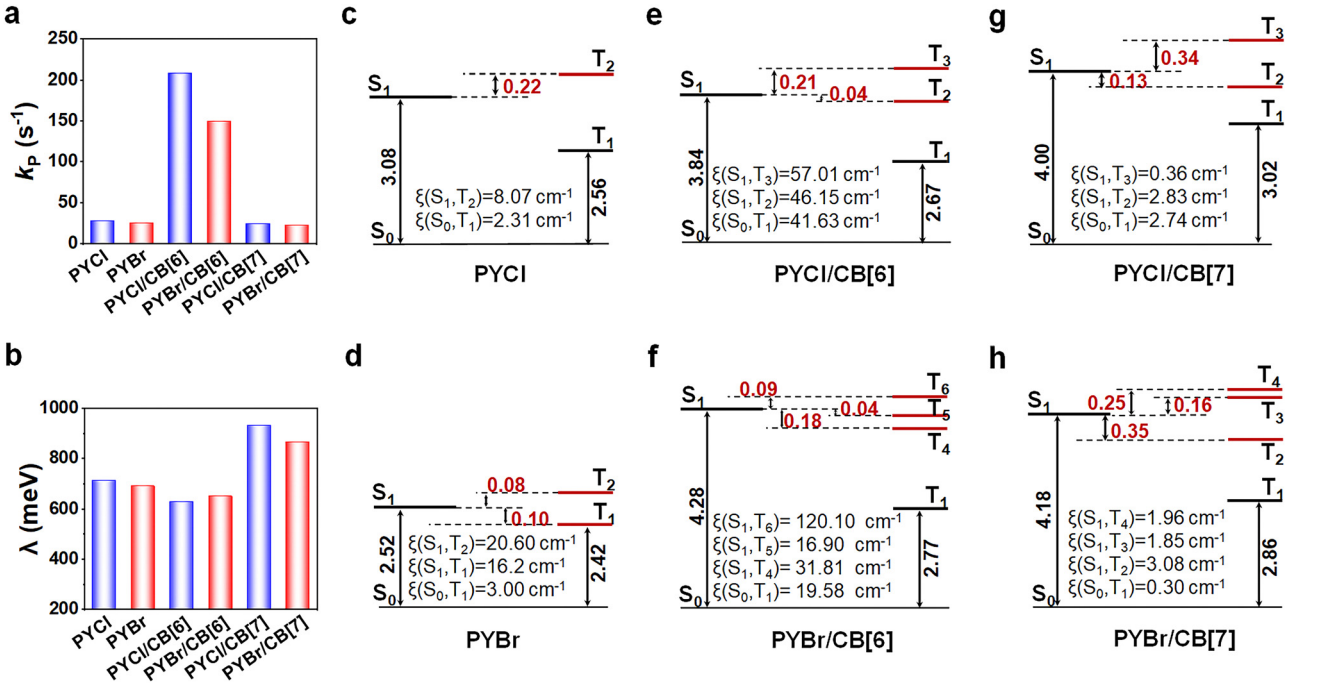

Fig. 5 (a) Phosphorescence radiative rate constant (k_P). (b) The λ calculated by the AP method of the studied molecules. (c)–(h) Calculated energy level based on BMK/6-31G** and the corresponding spin–orbital coupling SOC (ξ) of the studied molecules. The energy differences (ΔE_{ST}) and the excitation energies, in units of eV.

decay process. For the guests, λ of PYBr was slightly lower than that of PYCl (Fig. 5b). Upon complexation with CB[6], λ of both PYCl and PYBr decreased, while the λ increased when binding to CB[7] (Fig. 5b), consistent with the RMSD analysis discussed above. Therefore, the intramolecular vibrations of both PYCl and PYBr were largely restricted after complexation with CB[6] by host–guest interactions.

The ISC process is another crucial factor in phosphorescent emission. It is affected by two key parameters: SOC constant and energy gap between S_1 and T_n (ΔE_{ST}). Both the increases of SOC and the decrease of ΔE_{ST} are beneficial for the ISC process. According to the energy gap law,[56] the ISC channel with ΔE_{ST} lower than 0.37 eV is effective. From PYCl to PYBr, the ΔE_{ST} decreases from 0.22 eV to 0.08 eV, along with the SOC constant increasing from 8.07 cm^{-1} to 20.60 cm^{-1}, see Fig. 5c and d. Thus, the ISC process was effectively promoted from PYCl to PYBr, due to the introduction of heavy halogen atoms.[57] After complexation with CB[6], the populations of the triplet excitons and ISC channels improved efficiently. Taking PYCl and PYCl/CB[6] as examples, it can be seen that there are more effective ISC channels from S_1 to high-lying triplet excited states (T_2 and T_3) bearing ΔE_{ST} within 0.25 eV ($\Delta E_{S_1-T_3}$ = 0.21 eV, $\Delta E_{S_1-T_2}$ = 0.04 eV). These ISC channels also have larger SOC constants ($\xi_{S_1-T_3}$ = 57.01 cm^{-1}, $\xi_{S_1-T_2}$ = 46.15 cm^{-1}). Meanwhile, the SOC values of $\xi_{S_0-T_1}$ were enlarged from 2.31 cm^{-1} of PYCl to 41.63 cm^{-1} of PYCl/CB[6], facilitating the ISC process (Fig. 5e–h). Similarly, PYBr/CB[6] also exhibits more and effective ISC channels than that of PYBr. In contrast, the SOC of PYCl/CB[7] and PYBr/CB[7] are much smaller than those of the corresponding guests and CB[6]-type complexes (Fig. 5e–h), indicating that the introduction of CB[7] is less effective in facilitating the ISC process. According to the El-Sayed rule,[58] the different electronic configurations between singlet and triplet states are more favorable for the ISC process. As shown in Fig. S11 and S12 (ESI†), the transition nature of the S_1 state of PYCl is (n, π^*), and its T_1 and T_2 states are also predominantly (n, π^*), which is not favorable to the ISC process and leads to inefficient SOC. The transition nature of the S_1 state of PYCl/CB[6] is (π, π^*), however, the transition nature of T_2 and T_3 is dominated by (n, π^*), the different transition nature is beneficial for the ISC process and leads to efficient SOC. The (π, π^*) nature of S_1 of the PYBr/CB[6] facilitates the ISC process from S_1 to high-lying triplet states T_2 and T_5 in (n, π^*) character with close energy levels, reflected by the large SOC constants in PYBr/CB[6]. While the CB[7]-type host–guest complexes exhibit little difference between their S_1 and triplet states (Fig. S13, ESI†), leading to low SOC constants.

Above all, the PQY of PYBr should be higher than that of PYCl, because of the more favorable ISC process by the introduction of heavy atoms. The PQY of CB[6]-type host–guest complexes are greatly improved compared to those of pure guests, cooperatively attributed to the improvement of radiative transition and ISC processes from S_1 to low-lying triplet states, as well as suppressed non-radiative decay processes. While complexation with CB[7], the PQY are almost similar to those of pure guests. It indicates that the enhancement of phosphorescence only occurs in the CB[6]-type host–guest complexes, owing to the strong host–guest interactions. The cavity size of CB[6] can fit perfectly with PYCl and PYBr, and then form stable host–guest complexes, while the host–guest interactions of CB[7]-type complexes are relatively weak.

Conclusions

In summary, the mechanism of host–guest interaction-induced RTP enhancement was investigated by a multiscale modeling protocol based on the QM/MM model. It can be found that for two organic dyes, the better RTP performance of PYBr than PYCl is due to the favorable ISC process induced by the heavy atom effect. The heavy halogen Br^- of PYBr triggers a striking SOC and the small ΔE_{ST}, which is beneficial for promoting ISC. Notably, when two organic dyes bind to CB[6] through the host–guest interaction, they can accelerate the radiative transition by increasing the transition dipole moment of $T_1 \rightarrow S_0$ ($\mu_{T_1 \rightarrow S_0}$), block the non-radiative decay pathway, as well as promote the ISC process, eventually leading to a remarkably boosted RTP. Upon complexation, a strong hydrogen-bond network between organic dyes and CB[6] was formed, which activated an efficient radiative pathway from T_1 to S_0 by converting S_1 from $^1(n, \pi^*)$ in organic dyes to $^1(\pi, \pi^*)$ in the CB[6]-type host–guest complexes and made the significant enhancement in $\mu_{T_1 \rightarrow S_0}$, which greatly facilitates the radiative transition process. Moreover, strong host–guest interaction can lead to small reorganization energy and effectively suppress the non-radiative decay process by restricting the rotation of rings A and B in organic dyes. Simultaneously, the ISC process was significantly promoted due to more effective ISC channels between S_1 and high-lying triplet states, with a significant increase of SOC constants and a reduction in ΔE_{ST}. Conversely, the case of CB[7] is much different due to the weak host–guest interactions in the large cavity of CB[7], the large reorganization energy reflects the easy dissipation of excited energy through the non-radiative decay process. Furthermore, the phosphorescence emission of the host–guest complexes was red-shifted relative to that of the pure guests, which reproduced the spectral trend observed in the experiments. The red-shifted spectrum of the host–guest complexes was attributed to the reduced HOMO–LUMO energy gap at T_1. Our work sheds light on the intrinsic mechanism of enhancing the solid-state RTP induced by host–guest interaction. It provides systematic insights into the structure–property relationship of the RTP materials based on macrocyclic hosts, paving the way for the rational design of advanced RTP materials.

Conflicts of interest

The authors declare that there is no conflict of interest.

Acknowledgements

We thank the financial support of the National Natural Science Foundation of China (Grant 22173006), and Beijing Natural Science Foundation (Grant 2222027).

References

1 L. Dou, J. You, Z. Hong, Z. Xu, G. Li, R. A. Street and Y. Yang, *Adv. Mater.*, 2013, **25**, 6642–6671.
2 R. Kabe, N. Notsuka, K. Yoshida and C. Adachi, *Adv. Mater.*, 2016, **28**, 655–660.
3 W. Song and J. Y. Lee, *Adv. Opt. Mater.*, 2017, **5**, 1600901.
4 G. Zhang, G. M. Palmer, M. W. Dewhirst and C. L. Fraser, *Nat. Mater.*, 2009, **8**, 747–751.
5 S. M. A. Fateminia, Z. Mao, S. Xu, Z. Yang, Z. Chi and B. Liu, *Angew. Chem., Int. Ed.*, 2017, **56**, 12160–12164.
6 S. Cai, H. Shi, J. Li, L. Gu, Y. Ni, Z. Cheng, S. Wang, W.-W. Xiong, L. Li, Z. An and W. Huang, *Aggregate*, 2017, **29**, 1701244.
7 H. Qi, C. Chang and L. Zhang, *Green Chem.*, 2009, **11**, 177–184.
8 H. Ding, Y. Sun, M. Tang, J. Wen, S. Yue, Y. Peng, F. Li, L. Zheng, S. Wang, Y. Shi and Q. Cao, *Chem. Sci.*, 2023, **14**, 4633–4640.
9 Y. Su, S. Z. F. Phua, Y. Li, X. Zhou, D. Jana, G. Liu, W. Q. Lim, W. K. Ong, C. Yang and Y. Zhao, *Sci. Adv.*, 2018, **4**, eaas9732.
10 T. Zhang, J. Zhou, H. Li, J. Ma, X. Wang, H. Shi, M. Niu, Y. Liu, F. Zhang and Y. Guo, *Green Chem.*, 2023, **25**, 1406–1416.
11 X. Wei, J. Yang, L. Hu, Y. Cao, J. Lai, F. Cao, J. Gu and X. Cao, *J. Mater. Chem. C*, 2021, **9**, 4425–4443.
12 S. Datta and J. Xu, *ACS Appl. Bio Mater.*, 2023, **6**, 4572–4585.
13 F. Peng, Y. Chen, H. Liu, P. Chen, F. Peng and H. Qi, *Adv. Mater.*, 2023, **35**, 2304032.
14 A. Köhler and H. Bässler, *Mater. Sci. Eng., R*, 2009, **66**, 71–109.
15 S. Menning, M. Krämer, B. A. Coombs, F. Rominger, A. Beeby, A. Dreuw and U. H. F. Bunz, *J. Am. Chem. Soc.*, 2013, **135**, 2160–2163.
16 Z. Yang, C. Xu, W. Li, Z. Mao, X. Ge, Q. Huang, H. Deng, J. Zhao, F. L. Gu, Y. Zhang and Z. Chi, *Angew. Chem., Int. Ed.*, 2020, **59**, 17451–17455.
17 M. Shimizu, R. Shigitani, M. Nakatani, K. Kuwabara, Y. Miyake, K. Tajima, H. Sakai and T. Hasobe, *J. Phys. Chem. C*, 2016, **120**, 11631–11639.
18 A. Fermi, G. Bergamini, M. Roy, M. Gingras and P. Ceroni, *J. Am. Chem. Soc.*, 2014, **136**, 6395–6400.
19 C. Zhou, S. Zhang, Y. Gao, H. Liu, T. Shan, X. Liang, B. Yang and Y. Ma, *Adv. Funct. Mater.*, 2018, **28**, 1802407.
20 Y. Tian, Y. Gong, Q. Liao, Y. Wang, J. Ren, M. Fang, J. Yang and Z. Li, *Cell. Rep. Phys. Sci.*, 2020, **1**, 100052.
21 Z. An, C. Zheng, Y. Tao, R. Chen, H. Shi, T. Chen, Z. Wang, H. Li, R. Deng, X. Liu and W. Huang, *Nat. Mater.*, 2015, **14**, 685–690.
22 J. Wang, Z. Huang, X. Ma and H. Tian, *Angew. Chem., Int. Ed.*, 2020, **59**, 9928–9933.
23 J. Wei, B. Liang, R. Duan, Z. Cheng, C. Li, T. Zhou, Y. Yi and Y. Wang, *Angew. Chem., Int. Ed.*, 2016, **55**, 15589–15593.
24 H. Mieno, R. Kabe, N. Notsuka, M. D. Allendorf and C. Adachi, *Adv. Opt. Mater.*, 2016, **4**, 1015–1021.
25 Z.-Y. Zhang and Y. Liu, *Chem. Sci.*, 2019, **10**, 7773–7778.
26 W. Zhu, H. Xing, E. Li, H. Zhu and F. Huang, *Macromolecules*, 2022, **55**, 9802–9809.
27 Y. Zhou, D. Zhao, Z.-Y. Li, G. Liu, S.-H. Feng, B.-T. Zhao and B.-M. Ji, *Dyes Pigm.*, 2021, **195**, 109725.

28 N. J. Turro, J. D. Bolt, Y. Kuroda and I. Tabushi, *Photochem. Photobiol.*, 1982, **35**, 69–72.
29 L. Mu, X.-B. Yang, S.-F. Xue, Q.-J. Zhu, Z. Tao and X. Zeng, *Anal. Chim. Acta*, 2007, **597**, 90–96.
30 D. Li, F. Lu, J. Wang, W. Hu, X.-M. Cao, X. Ma and H. Tian, *J. Am. Chem. Soc.*, 2018, **140**, 1916–1923.
31 Z. Y. Zhang, Y. Chen and Y. Liu, *Angew. Chem., Int. Ed.*, 2019, **58**, 6028–6032.
32 H. Ma, W. Shi, J. Ren, W. Li, Q. Peng and Z. Shuai, *J. Phys. Chem. Lett.*, 2016, **7**, 2893–2898.
33 H. Ma, Q. Peng, Z. An, W. Huang and Z. Shuai, *J. Am. Chem. Soc.*, 2019, **141**, 1010–1015.
34 Q. Mu, K. Zhang, H. Zou, H. Liu, Y. Song, C.-K. Wang, L. Lin and J. Fan, *Dyes Pigm.*, 2022, **205**, 110560.
35 Y. Wang, Q. Peng and Z. Shuai, *Mater. Horiz.*, 2022, **9**, 334–341.
36 B. Li, Y. Gong, L. Wang, H. Lin, Q. Li, F. Guo, Z. Li, Q. Peng, Z. Shuai, L. Zhao and Y. Zhang, *J. Phys. Chem. Lett.*, 2019, **10**, 7141–7147.
37 J. Kim, I.-S. Jung, S.-Y. Kim, E. Lee, J.-K. Kang, S. Sakamoto, K. Yamaguchi and K. Kim, *J. Am. Chem. Soc.*, 2000, **122**, 540–541.
38 S. Grimme, *J. Comput. Chem.*, 2006, **27**, 1787–1799.
39 G. Kresse and J. Furthmüller, *Phys. Rev. B: Condens. Matter Mater. Phys.*, 1996, **54**, 11169–11186.
40 M. J. Frisch, G. W. Trucks, H. B. Schlegel, G. E. Scuseria, M. A. Robb, J. R. Cheeseman, G. Scalmani, V. Barone, G. A. Petersson, H. Nakatsuji, X. Li, M. Caricato, A. V. Marenich, J. Bloino, B. G. Janesko, R. Gomperts, B. Mennucci, H. P. Hratchian, J. V. Ortiz, A. F. Izmaylov, J. L. Sonnenberg Williams, F. Ding, F. Lipparini, F. Egidi, J. Goings, B. Peng, A. Petrone, T. Henderson, D. Ranasinghe, V. G. Zakrzewski, J. Gao, N. Rega, G. Zheng, W. Liang, M. Hada, M. Ehara, K. Toyota, R. Fukuda, J. Hasegawa, M. Ishida, T. Nakajima, Y. Honda, O. Kitao, H. Nakai, T. Vreven, K. Throssell, J. A. Montgomery Jr., J. E. Peralta, F. Ogliaro, M. J. Bearpark, J. J. Heyd, E. N. Brothers, K. N. Kudin, V. N. Staroverov, T. A. Keith, R. Kobayashi, J. Normand, K. Raghavachari, A. P. Rendell, J. C. Burant, S. S. Iyengar, J. Tomasi, M. Cossi, J. M. Millam, M. Klene, C. Adamo, R. Cammi, J. W. Ochterski, R. L. Martin, K. Morokuma, O. Farkas, J. B. Foresman and D. J. Fox, *Gaussian 16, Revision A.03*, Gaussian Inc., Wallingford, CT, 2016.
41 J. Tao, J. P. Perdew, V. N. Staroverov and G. E. Scuseria, *Phys. Rev. Lett.*, 2003, **91**, 146401.
42 S. Grimme, J. Antony, S. Ehrlich and H. Krieg, *J. Chem. Phys.*, 2010, 132.
43 A. D. Boese and J. M. L. Martin, *J. Chem. Phys.*, 2004, **121**, 3405–3416.
44 Y. Zhao and D. G. Truhlar, *Theor. Chem. Acc.*, 2008, **120**, 215–241.
45 A. K. Rappe, C. J. Casewit, K. S. Colwell, W. A. Goddard, III and W. M. Skiff, *J. Am. Chem. Soc.*, 1992, **114**, 10024–10035.
46 Y. Zeng, W. Shi, Q. Peng, Y. Niu, Z. Ma and X. Zheng, *Phys. Chem. Chem. Phys.*, 2024, **26**, 1303–1313.
47 D. Bakowies and W. Thiel, *J. Phys. Chem.*, 1996, **100**, 10580–10594.
48 C. I. Bayly, P. Cieplak, W. Cornell and P. A. Kollman, *J. Phys. Chem.*, 1993, **97**, 10269–10280.
49 Q. Peng, Y. Niu, Q. Shi, X. Gao and Z. Shuai, *J. Chem. Theory Comput.*, 2013, **9**, 1132–1143.
50 K. Aidas, C. Angeli, K. L. Bak, V. Bakken, R. Bast, L. Boman, O. Christiansen, R. Cimiraglia, S. Coriani, P. Dahle, E. K. Dalskov, U. Ekström, T. Enevoldsen, J. J. Eriksen, P. Ettenhuber, B. Fernández, L. Ferrighi, H. Fliegl, L. Frediani, K. Hald, A. Halkier, C. Hättig, H. Heiberg, T. Helgaker, A. C. Hennum, H. Hettema, E. Hjertenæs, S. Høst, I.-M. Høyvik, M. F. Iozzi, B. Jansík, H. J. A. Jensen, D. Jonsson, P. Jørgensen, J. Kauczor, S. Kirpekar, T. Kjærgaard, W. Klopper, S. Knecht, R. Kobayashi, H. Koch, J. Kongsted, A. Krapp, K. Kristensen, A. Ligabue, O. B. Lutnæs, J. I. Melo, K. V. Mikkelsen, R. H. Myhre, C. Neiss, C. B. Nielsen, P. Norman, J. Olsen, J. M. H. Olsen, A. Osted, M. J. Packer, F. Pawlowski, T. B. Pedersen, P. F. Provasi, S. Reine, Z. Rinkevicius, T. A. Ruden, K. Ruud, V. V. Rybkin, P. Sałek, C. C. M. Samson, A. S. de Merás, T. Saue, S. P. A. Sauer, B. Schimmelpfennig, K. Sneskov, A. H. Steindal, K. O. Sylvester-Hvid, P. R. Taylor, A. M. Teale, E. I. Tellgren, D. P. Tew, A. J. Thorvaldsen, L. Thøgersen, O. Vahtras, M. A. Watson, D. J. D. Wilson, M. Ziolkowski and H. Ågren, *WIREs Comput. Mol. Sci.*, 2014, **4**, 269–284.
51 F. Neese, *WIREs Comput. Mol. Sci.*, 2012, **2**, 73–78.
52 T. Zhang, Y. Jiang, Y. Niu, D. Wang, Q. Peng and Z. Shuai, *J. Phys. Chem. A*, 2014, **118**, 9094–9104.
53 T. Lu and F. Chen, *Acta Chim. Sin.*, 2011, **69**, 2393–2406.
54 Y. Zeng, J. M. Qu, G. H. Wu, Y. Y. Zhao, J. M. Hao, Y. P. Dong, Z. S. Li, J. B. Shi, J. S. Francisco and X. Y. Zheng, *J. Am. Chem. Soc.*, 2024, **146**(14), 9888–9896.
55 A. Lv, Z. Yu, Y. Mao, X. Zheng, W. Shi, H. Shi, W. Yao, H. Ma and Z. An, *Dyes Pigm.*, 2021, **193**, 109520.
56 Y. Tao, K. Yuan, T. Chen, P. Xu, H. Li, R. Chen, C. Zheng, L. Zhang and W. Huang, *Adv. Mater.*, 2014, **26**, 7931–7958.
57 H. Shi, Z. An, P.-Z. Li, J. Yin, G. Xing, T. He, H. Chen, J. Wang, H. Sun, W. Huang and Y. Zhao, *Cryst. Growth Des.*, 2016, **16**, 808–813.
58 M. A. El-Sayed, *Acc. Chem. Res.*, 1968, **1**, 8–16.

